RSC Advances

ROYAL SOCIETY OF CHEMISTRY

www.rsc.org/advances

Journal Name

RSCPublishing

ARTICLE

π-π Interactions Mediated Self-Assembly of Gold Nanoparticles into Single Crystalline Superlattices in Solution†

Cite this: DOI: 10.1039/x0xx00000x

Received 00th January 2012,
Accepted 00th January 2012

DOI: 10.1039/x0xx00000x

www.rsc.org/

FuKe Wang,*[a] Yuriy A. Akimov,[b] Khoo Eng Huat[b] and Chaobin He*[a,c]

A first attempt of employing π-π interaction for self-assembly of colloidal gold nanoparticles into 3D single crystalline superlattices in solution is presented. It is demonstrated that simple capping ligands exchange with aromatic thiols leads to self-assembly of gold nanoparticles into *fcc* packed superlattices with well-defined facets and long-range ordering. Stimuli that can break the π-π interactions lead to disassembly of gold nanoparticles, allowing the design of reversible assembly and reconfiguration. The crystallization of gold nanoparticles is shown to be kinetically controlled by the concentration of aromatic thiols in solution, enabling efficient tuning of the long- and short-range ordering in nanoparticles lattices, accompanied with corresponding changes of the effective optical properties.

Introduction

Nanomaterial research has received global attention in the past few decades. Various nanomaterials with different structural features and sizes, together with different composition including metals, semiconductors, oxides, carbide, organic and polymers have been prepared to give impetus to new applications.[1] With the development of nanomaterials research, it has been recognized that assembly of nanoparticles into macroscopic architectures can result in enhanced optical, electronic, magnetic, and catalytic properties.[2] Importantly, many researches have pointed out that the ordering and packing of nanoparticles (NPs) in the assembly is of utmost importance for the development of materials with unique properties.[3] Therefore, superlattices of colloidal NPs emerged as a new class of building blocks in nanofabrication to construct cost-effectively NPs-based devices through bottom-up, solution processing approaches.[4] Many applications such as biomedical diagnosis, catalysis, plasmonics, high-density data storage, and energy conversion have been reported by using NPs assemblies.[5] In addition, NPs assembly follows a similar crystallization principle of atoms and molecules. Therefore, the self-assembly of NPs into colloidal crystal provides a unique opportunity to study the general aspects of crystallization process by using either real-space imaging technique or in situ monitoring of optical and electronic properties.[6]

Many approaches have been explored to mediate assembly of different NPs.[7] Among these researches, gold (Au) NPs received much more attention due to easy synthesis and size control, as well as for their unique plasmonic properties.[8] Most of Au NPs assembly studies led to the formation of two-dimensional (2D) assembly or three-dimensional (3D) amorphous aggregates.[9] The difficulty in achieving well-defined crystalline superlattices resides in the efficient control over particle-particle interaction and coalescence dynamics.[10] Currently, Au NPs superlattices (crystals) are mainly produced by slow and controlled solvent evaporation of Au NPs suspension with a narrow size distribution, where assembly is driven by minimization of the surface energy via elimination of interfaces. As this approach is based on solvent evaporation, it naturally lacks control over the crystals size and structure, as well as the difficulty in reconfiguration of NPs through reversible disassembly.[11] To achieve a high level of control over the assembly to form macroscopic structure in solution, DNA-mediated crystallization of Au NPs was proposed as a first attempt for the chemically induced self-assembly. It provides high selectivity for nanocrystals' sizes and inter-particles distance through precise recognition of complementary DNA strands via hydrogen bonding. However, the DNA-guided crystallization needs tedious NPs surface functionalization together with repeat heating/cooling cycles to facilitate the formation of face-centered cubic (*fcc*) and body-centered cubic (*bcc*) crystal structures.[12]

In this paper, we report a facile way to create a single crystalline Au NPs superlattice in solution by employing π-π interactions in a controlled manner. Theoretical and empirical studies have shown that aromatic rings tend to form higher-order clusters driven by entropy.[13] In this study, we demonstrate that addition of aromatic thiols to Au NPs leads to the formation of *fcc* packed Au colloidal crystals. Interestingly, the π-π interactions mediated NPs assembly can be kinetically tailored to form short- and long-range ordered structures,

providing tunable physical properties of the resulting superlattice. Importantly, disassembly of the ordered superlattice can be simply achieved through breaking the π-π interactions, allowing the design of reversible assembly of Au NPs or their reconfiguration in response to external stimuli.

Results and Discussion

Fig. 1 shows a schematic illustration of the π-π interactions mediated crystallization of Au NPs in solution. Uniform sized Au NPs were first capped with oleylamine (OLA) and dispersed in an organic solution of hexane. When aromatic thiol ligand, 1-mercaptonaphthalene (NaphSH), was added to the solution, ligands exchange occurred on the surface of Au NPs due to the stronger Au-thiols interactions. The attractive nonbonded interactions between the naphthalene rings provide the driving force for gold NPs assembly. At the same time, the repulsive interactions between particles and solution media provide an environment that allows NPs to move and to adjust their positions with respect to others in solution.

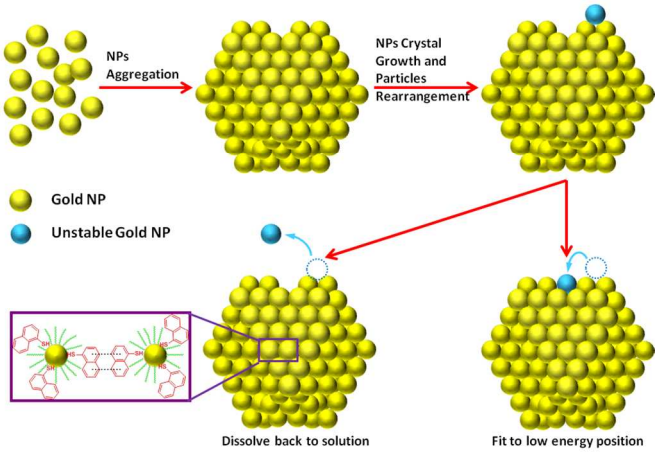

Fig. 1 Schematic illustration of π-π interactions mediated crystallization of Au NPs in solution. The ligands exchange of aromatic thiols with OLA on the surface of Au NPs causes the assembly of Au NPs mediated by π-π interactions. Unstable Au NPs either adjust their positions to the energy favorable positions or dissolve back to the solution.

In a typical experiment, uniform Au NPs with diameter of 11 ± 0.5 nm were synthesized by the reduction of $HAuCl_4$ in oleylamine solution at 80 °C for 4 hours. The obtained gold NPs were purified by precipitation into alcohol and centrifugation, washed with alcohol and re-dispersed in hexane to yield a homogeneous wine-red solution. The resulting oleylamine-capped gold NPs showed a strong local surface plasmon resonance (LSPR) at 520 nm. The concentration of gold NPs solution was measured by UV-vis spectra and determined based on the extinction coefficients method as reported.[14] Typically, the Au NPs solution in hexane was adjusted to about 1.1×10^{12} NPs/ml (about 7.5×10^{-5} mol/L based Au element) before assembly. Under continue shaking or stirring, NaphSH was added to Au NPs solution to reach the final concentration of 5 mmol/L at room temperature. The solution displayed a gradual color change from red to blue and finally to grey in about 45 min after addition of NaphSH to gold NPs solution in hexane.

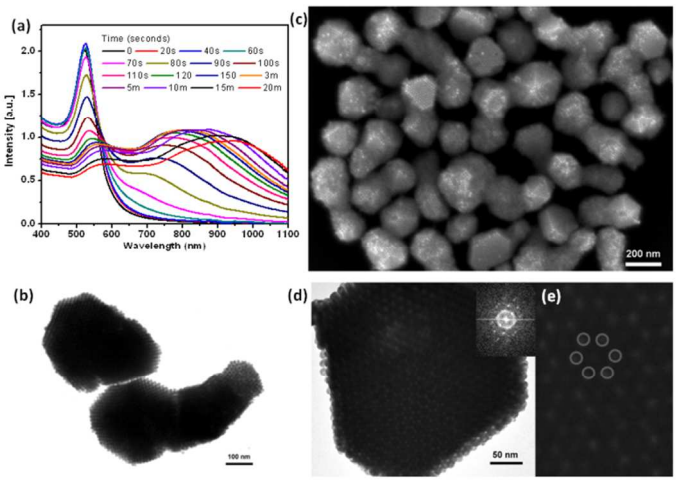

Fig. 2 3D Au NPs superlattices in hexane solution. (a) The UV-vis-NIR extinction spectra evolution as function of time in 5 mM of NaphSH hexane solution. (b) TEM images of formed 3D Au NPs superlattices. (c) SEM images of the formed single crystalline superlattices with defined faceted surfaces. (d) High resolution TEM analysis of the formed single crystalline Au NPs superlattices. Inset shows the FFT image of the crystal displayed in (d). (e) Hexagonal arranged voids show the face-centered closely packed NPs superlattices.

Color change of the solution was accompanied with the gradual variation of the spectral extinction as shown in Fig. 2a. There was nearly no obvious spectra change at the early stage. However, after 70 seconds, a shoulder peak appeared at longer wavelength (660 nm) together with bleaching of the LSPR at 520 nm. The remarkable spectral change occurred at the second minute, when the long-wavelength peak shifted from 700 nm to 800 nm. Within next 20 mins, the long-wavelength peak was further shifted to about 980 nm, together with a gradual red-shift and bleaching of LSPR. Finally, two peaks were stabilized at around 570 and 980 nm. The formed Au NPs assembles were then purified by low speed centrifugation and re-dispersed into hexane.

The highly ordered packing of Au NPs was confirmed by transmission electron microscopy (TEM) analysis shown in Fig. 2b. The formed superlattices were found to be polyhedrons rather than spheres, with sizes ranged from 200 to 300 nm. The formation of well-faceted superlattices was further confirmed by scanning electron microscope (SEM) analysis as shown in Fig. 2c. It revealed that the formed assemblies are single crystalline with highly ordered 3D packing of Au NPs. The flat facets of crystals are composed by closely packed nanoparticles in the manner of ABCABC stacking. Small-angle X-ray diffraction (SAXS) patterns of these superlattices (see ESI, Fig. S1†) indicates that gold NPs were assembled into an *fcc* structure with lattice parameter of a = 19.6 nm. The packing model of gold NPs was further studied by using high magnification TEM and fast Fourier transform (FFT) analysis. TEM analysis showed that the assembled gold NPs exhibit on-axis superlattices-fringe patterns attributed to an *fcc* superlattices structures (Fig. 2d,e). As shown in Fig. 2d, the [111] projection image exhibits the characteristics of long-range *fcc* ordering of the individual nanocrystals with

hexagonal cross-fringes. The cross-fringes in the [001] and [011] projection image and patterns (see ESI, Fig. S2†) also confirmed the formation of *fcc* superlattices structures.

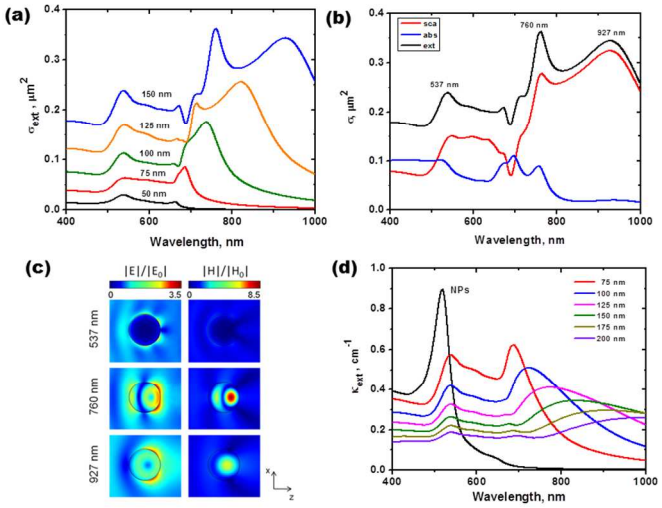

Fig. 3 Simulation results for the Au NPs superlattices. (a) Extinction cross-sections of the effective spherical aggregates with different values of the radius R. (b) Contributions of scattering and absorption to the extinction cross-sections of the effective sphere of R=150 nm. (c) Spatial distribution of the electric and magnetic fields around the effective sphere of R=150 nm at the three peak wavelengths of 537, 760, and 927 nm. (d) Spectral dependence of the statistical extinction coefficient for the populations of spherical aggregates obeying the truncated normal distribution with six different values of the mean radius R_0. The standard deviations are assumed to be $\Delta R = 0.2\ R_0$, with the fixed density of the Au NPs $n_0 = 1.1 \times 10^{12}$ NPs/ml. The curve labeled "NPs" shows the extinction coefficient of NPs before assembly.

To gain insight into the origins of the long-wavelength extinction of the self-assembled Au NPs crystals, optical properties of Au NPs superlattice were calculated by solving the full set of 3D Maxwell's equations for the infinitely long (in the x- and y-directions) structure consisting of five identical layers of the *fcc*-packed NPs (see ESI, Fig. S3†). Although, the actual shape of the observed crystalline aggregates is polyhedral rather than spherical, effective spheres are still a good model to study the assemblies' spectral extinction (see ESI, Fig. S4†), as the extinction measurements were taken for the aggregates moving in the solution. The extinction cross-sections of effective spheres were calculated using the Mie theory[15] and are shown in Fig. 3a for different values of the radius. Following this theory, the extinction cross-sections are particularly sensitive to the aggregates size. Fig. 3a clearly demonstrates the difference in extinction by small and large assemblies – for small aggregates, the strong short wavelength extinction is observed governed by the LSPR in Au NPs, while for larger aggregates, a longer wavelength extinction appears in addition to the LSPR that becomes dominant with the growth of the assemblies. Moreover, as the size of aggregates increases, more peaks appear in the long-wavelength range given by the enhanced scattering of light, as shown in Fig. 3b. This enhancement originates from the constructive interference of light on a dielectric sphere,[15,16] confirmed by the dominating scattering (Fig. 3b) and the interference patterns of the electric and magnetic fields in a sphere (Fig. 3c). Thus, the scattering enhanced by bigger assemblies increases the extinction of incident light in the long-wavelength range. Eventually, after mixing of aggregates with different size and statistical averaging of their cross-sections, the extinction peak shifts towards longer wavelength, getting broader and less pronounced, as shown in Fig. 3d.

The performed analysis of exctinction reveals that the long-wavelength peak appeared in the UV-vis-NIR spectra is a statistically blurred interference-induced resonance, governed by the aggregates size distribution. As a result, it can be directly used for estimation of the aggregates size distribution (Fig. 3d). This enables us to interpret temporal evolution of the extinction spectra in terms of the assembly dynamics for in situ characterization and study of the crystallization process (see ESI, Fig. S5†).

As the NPs assembly is attributed to the π-π interaction, self-organization dynamics is very sensitive to the properties of the capping ligands.[17] Due to stronger interaction of Au-thiol than Au-NH_2, it is reasonable to expect that NaphSH will replace OLA to form new capping ligands on Au NPs surface, when NaphSH is added to the solution. This was confirmed by nuclear magnetic resonance (NMR) spectroscopy analysis of the free gold NPs and assembled gold NPs (see ESI, Fig. S6†). NMR analysis of free gold NPs showed only signal from OLA, while NMR spectra of assembled gold NPs exhibited both peaks from OLA and NaphSH. Integration of the peaks of assembled gold NPs showed that nearly half of OLA was substituted by NaphSH at a low thiols concentration (5 mmol/L), suggesting strong interaction of NaphSH with NPs surface. The capping of Au NPs surface with NaphSH leads to a substantial increase in the attraction potential between nanoparticles and results in their assembly.

Notably, π-π interaction force is within the range of 8-12 kJ/mol,[18] which is weaker than the hydrogen bonds used in the DNA-mediated Au NPs assembly. Thus, no extra energy is required for NPs motion within an aggregate once it has been assembled, to adjust their position and form single crystalline superlattices. Therefore, in our approach, the tedious repeated heating/cooling cycles, which are traditionally used in the DNA-mediated assembly to reach low energy structures, can be avoided. As a result, the assembly of high-ordered structures can be achieved in a shorter time. In addition, the solution, where the assembly occurs, provides the enviroment for Au NPs to adjust their unfavor position and form more stable superlattices. Thereafter, the combination of π-π interaction and solution assembly prevent the unlimited growth of particles aggregates and short-range ordering, which often occurs in other assembly techniques. Furthermore, assembly in solution provides a great opportunity for in situ monitoring of the dynamic crystallation process. The three basic crystallization steps including nucleation, fast growth, and equilibrium can be seen directly in the time-function UV-vis spectra. It gives a metrology for in situ kinetics characterization and helps in studying fundamental aspects of crystallization.

Similar to the molecular crystallization, the structure and shape of the Au NPs aggregates are under kinetic control. As shown in Fig. 4a, when Au NPs were assembled in the presence of higher concentration of NaphSH (12.5 mmol/L), a quick aggregation was observed through fast solution color change

and the corresponding UV-vis extinction spectra. As shown in Fig. 4a, LSPR of Au NPs red-shifted together with rapid appearance of the long-wavelength peak upon addition of high concentrated NaphSH (12.5 mM). The newly formed peak quickly stabilized at 830 nm, suggesting a short-range coupling of Au NPs with smaller mean size of assemblies. The formed gold NPs aggregates were characterized by TEM, which showed short-range packing of Au NPs and smaller sizes of the aggregates.

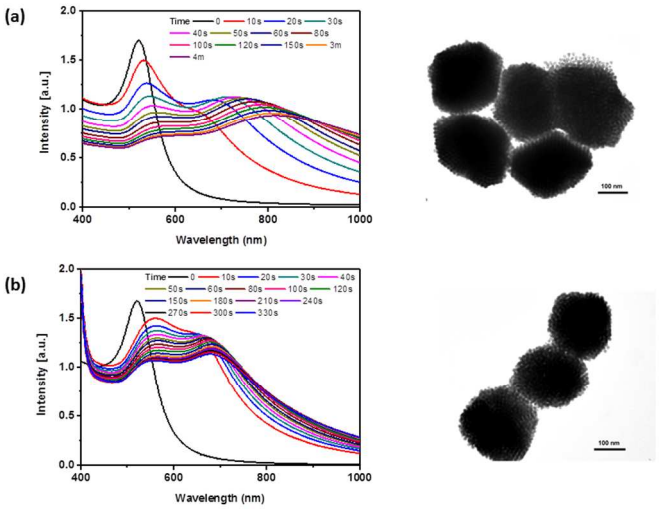

Fig. 4 Chemically controlled Au NPs aggregates with long- and short-range ordered assembly. (a) The UV-vis extinction evolution versus time in 12.5 mM of NaphSH hexane solution (left) and TEM images of formed Au NPs assembles (right). (b) The UV-vis extinction evolution versus time in 200 mM of NaphSH hexane solution (left) and TEM images of the formed Au NPs assembles (right).

Further increase of NaphSH concentration leads to the formation of random Au NPs aggregates. Fig. 4b shows one example of Au NPs assembly in 200 mmol/L NaphSH solution. Au NPs started to aggregate immediately upon addition of the high concentration NaphSH. The solution color changed to blue quickly and the long-wavelength extinction peak appeared at about 680 nm. Further assembly led only to a slight decrease of the LSPR intensity and broadening of the long-wavelength peak. TEM analysis of the formed Au NPs aggregates showed the formation of monodispersed amorphous spheres with size changing from 150 nm to 200 nm. This suggests that the assembly of Au NPs in the presence of NaphSH is a kinetic controlled process that provides a simple way to tune the aggregates' extinction: lower concentration of NaphSH causes long-ordered assembly, while higher concentration of NaphSH results in short-range ordering of Au NPs.

The NaphSH concentration-induced short- and long-range ordering was attributed to the different NPs self-organization mechanisms. As we have discussed above, single crystalline superlattices were formed at low NaphSH concentration because Au NPs assembly was dominated by π-π interactions. However, at higher NaphSH concentration, Au NPs assembly was mainly driven by the depletion force created by the large amount of free NaphSH in the solution.[19] The depletion force pushes Au NPs to aggregate quickly. As a result of the fast aggregation, Au NPs do not have enough time to re-arrange their positions in the formed nanocrystals, and thus lead to short-range coupling with more amorphous assemblies. Also, due to the fast nucleation, large amount of nucleus formed at the early stage, leading to the formation of smaller amorphous aggregates in the solution.

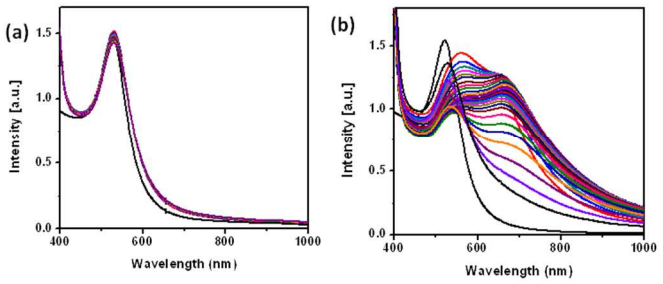

Fig. 5 Mechanism studies of the π-π interactions-mediated crystallization of Au NPs. (a) Extinction spectrum change of Au NPs in toluene upon addition of NaphSH (5 mmol/L) from time 0 to 5 min. (b) Extinction change of Au NPs in hexane with addition of high concentrated NaphSH (300 mmol/L) from time 0 to 5 min.

To have a better understanding of the π-π interaction in Au NPs assembly, several control experiments were carried out. Firstly, since the π-π stacking provides the driving force for Au NPs ordered assembly, any disturbance of the π-π interaction should prevent the NPs assembly. To confirm this assumption, NaphSH-mediated Au NPs assembly was carried out in toluene solution. Toluene is mono-substituted benzene derivative and an aromatic hydrocarbon widely used as a solvent. In toluene solution, NaphSH mainly interacts with the solvent, preventing the π-π interaction of NPs. As shown in Fig. 5a, when NaphSH is added to Au NPs solution in toluene, no obvious extinction change is observed. It confirms that Au NPs are stable and no aggregation occurs in the solution. Subsequent TEM analysis did not show any 3D single crystals formed. In fact, disturbance of π-π interaction can also be observed in hexane solution at very high concentration of NaphSH. Upon addition of highly concentrated NaphSH (300 mM) to the Au NPs solution, aggregation of Au NPs is observed immediately, pushed by the depletion force and π-π interaction. Surprisingly, the formed Au NPs aggregates disassembled into free Au NPs again subsequently and made the solution color change from grey to red. The dynamic change can be seen clearly from the in situ UV-vis extinction spectra as shown in Fig. 5b. Upon addition of NaphSH, the interference-induced peak appears and then disappears, revealing early stage assembly and subsequent disassembly of NPs. Thus, disassembly of Au NPs aggregates (either with long-range or short-range ordering) can easily be achieved through simple chemical stimuli such as addition of highly concentrated aromatic thiols or toluene to disturb the π-π interactions.

Conclusions

In summary, we have showed that single crystalline Au NPs superlattices can be prepared in a simple way by realizing the π-π interaction-mediated self-assembly in NaphSH solution. The crystallization process can be directly monitored in-situ

through evolution of the UV-vis extinction spectrum featuring plasmonic properties of Au NPs. Both the extinction and TEM analyses confirmed the existence of long-range translational ordering of Au NPs in the resulting superlattice structures. Similar to the molecular crystallization, Au NPs self-assembly has been shown to be kinetically controlled by the concentration of the aromatic thiols in solution, resulting in long- or short-range ordered Au NPs aggregates. In addition, disassembly of both long- and short-range ordered Au NPs crystals can be stimulated by chemicals such as aromatic thiols and aromatic solvents through breaking of the π-π interactions. In contrast to the solvent evaporation technique, the π-π interaction-mediated assembly can achieve a higher-order single crystalline-like Au NPs supperlattice in solution with well-defined faceted structures, together with the ability to disassemble aggregates upon stimuli. Compared with the DNA-mediated technique, the given method avoids the tedious heating and cooling cycles to get the higher-order structures, as well as the use of enzymes to achieve the disassembly. Most importantly, the proposed method is very simple and does not require any highly specialized equipment or sophisticated techniques for its realization.

Acknowledgements

We acknowledge financial support of this work from the Science and Engineering Research Council (Grant 1325504107) of Agency for Science, Technology and Research of Singapore.

Notes and references

[a] Synthesis and Integration, Institute of Materials Research and Engineering, Agency for Science, Technology and Research (A*STAR), 3 Research Link, Singapore, 117602

[b] Electronics and Photonics, Institute of High Performance Computing, Agency for Science, Technology and Research (A*STAR), 1 Fusionopolis Way, #16-16 Connexis, Singapore 138632

[c] Department of Materials Science and Engineering, National University of Singapore, 9 Engineering Drive 1, Singapore 117576.

† Electronic Supplementary Information (ESI) available: Derail experiments procedures for gold nanoparticles synthesis, assembly, and optical properties stimulation, more FFT studies. See DOI: 10.1039/b000000x/

1 (a) P. D. Howes, R. Chandrawati and M. M. Stevens, *Science* 2014, **346**, 1247390; (b) M. Ibáñez and A. Cabot, *Science*, 2013, **340**, 935; (c) S. Salvatore, S. Vignolini, J. Philpott, M. Stefik, U. Wiesner, J. J. Baumberg and U. Steiner, *Nanoscale* 2015, **7**, 1032; (d) L. Sang, Y. Zhao and C. Burda, *Chem. Rev.*, 2014, **114**, 9283; (e) B. Gao, M. J. Rozin and A. R. Tao, *Nanoscale*, 2013, **5**, 5677.

2 (a) C. B. Murray, C. R. Kagan and M. G. Bawendi, *Ann. Rev. Mater. Sci*., 2000, **30**, 545; (b) S. –J. Park, A. Lazarides, C. A. Mirkin, P. Brazis, C. Kannewurf and R. Letsinger, *Angew. Chem. Int. Ed*., 2000, **39**, 3845; (c) E. M. Hicks, S. Zou, G. C. Schatz, K. G. Spears, R. P. Van Duyne, L. Gunnarsson, T. Rindzevicius, B. Kasemo, M. Käll, *Nano Lett*. 2005, **5**, 1065; (d) H. Li, H. Yu, L. Sun, J. Zhai and X. Han, *Nanoscale* 2015, **7**, 1610.

3 (a) I. Lisiecki, V. Halté, C. Petit, M-P. Pileni and J. Y. Bigot, *Adv. Mater*. 2008, **20**, 4176; (b) N. Zaitseva, Z. R. Dai, F. R. Leon and D. Krol, *J. Am. Chem. Soc*. 2005, **127**, 10221; (c) I. Lisiecki, D. Parker, C. Salzemann and M. P. PileniChem, *Chem. Mater*., 2007, **19**, 4030.

4 R. Klajn, K. J. M. Bishop, M. Fialkowski, M. Paszewski, C. J. Campbell, T. P. Gray and B. A. Grzybowski, *Science*, 2007, **316**, 261.

5 (a) T. C. Harman, P. Taylor, M. P. Walsh and B. E. LaForge, *Science*, 2002, **297**, 2229; (b) D. V. Talapin, J-S. Lee, M. V. Kovalenko and E. V. Shevchenko, *Chem. Rev*., 2010, **110**, 389.

6 (a) Z. L. Wang, *Adv. Mater*., 1998, **10**, 13; (b) S. M. Rupich, E. V. Shevchenko, M. I. Bodnarchuk, B. Lee and D. V. Talapin, *J. Am. Chem. Soc*., 2010, **132**, 289.

7 (a) R. J. Macfarlane, B. Lee, M. R. Jones, N. Harris, G. C. Schatz and C. A. Mirkin, *Science*, 2011, **334**, 204; (b) D. Nykypanchuk, M. M. Maye, D. van der Lelie and O. Gang, *Nature*, 2008, **451**, 549; (c) A. K. Boal, F. Ilhan, J. E. DeRouchey, T. Thurn-Albrecht, T. P. Russell and V. M. Rotello, *Nature*, 2000, **404**, 746; (d) Z. Nie, D. Fava, E. Kumacheva, S. Zou and G. C. Walker, *Nat. Mater*., 2007, **6**, 609; (e) S. A. Jenekhe and X. L. Chen, *Science*, 1998, **279**, 1903; (f) X. Zhang, J. Han, Y. Zhou, Y. Ning, J. Wu, S. Liang, H. Sun, H. Zhang and B. Yang, *J. Mater. Chem*., 2012, **22**, 2679; (g) C. J. Zhong and S. I. Lim, *Acc. Chem. Res*., 2009, **42**, 798.

8 (a) R. Sardar, A. M. Funston, P. Mulvaney and R. W. Murray, *Langmuir*, 2009, **25**, 13840; (b) C. Zhang, Y. Zhou, A. Merg, C. Song, G. C. Schatz and N. L. Rosi, *Nanoscale* 2014, **6**, 12328.

9 (a) T. Wang, D. LaMontagne, J. Lynch, J. Zhuang and Y. C. Cao, *Chem. Soc. Rev.*, 2013, **42**, 2804; (b) M. P. Pileni, *J. Mater. Chem*., 2011, **21**, 16748.

10 (a) S. Dhakal, K. L. Kohlstedt, G. C. Schatz, C. A. Mirkin and M. O. de la Cruz, *ACS Nano*, 2013, **7**, 10948; (b) M. Grzelczak, J. Vermant, E. M. Furst, L. M. Liz-Marzán, *ACS Nano*, 2010, **4**, 3591.

11 (a) S. Bao, J. Zhang, Z. Jiang, X. Zhou and Z. Xie, *J. Phys. Chem. Lett* 2013, **4**, 3440; (b) A. Sánchez-Iglesias, M. Grzelczak, T. Altantzis, B. Goris, J. Pérez-Juste, S. Bals, G. Van Tendeloo, S. H. Donaldson Jr., B. F. Chmelka, J. N. Israelachvili, L. M. Liz-Marzán, *ACS Nano* 2012, **6**, 11059; (c) N. Goubet, J. Richardi, P-A. Albouy, M-P. Pileni, *Adv. Funct. Mater*., 2011, **21**, 2693.

12 (a) C. A. Mirkin, R. L. Letsinger, R. C. Mucic and J. J. Storhoff, *Nature*, 1996, **382**, 607; (b) A. P. Alivisatos, K. P. Johnsson, X. Peng, T. E. Wilson, C. J. Loweth, M. P. Bruchez Jr and P. G. Schultz, *Nature*, 1996, **382**, 609.

13 (a) R. E. Gillard, F. M. Raymo and J. F. Stoddart, *Chem. Eur. J.*, 1997, **3**, 1933; (b) C. A. Hunter, *Angew. Chem. Int. Ed.*, 1993, **32**, 1584.

14 W. Haiss, N. T. K. Thanh, J. Aveyard and D. G. Fernig, *Anal. Chem.*, 2007, **79**, 4215.

15 J. A. Stratton, *Electromagnetic Theory*, McGraw-Hill Book Company. Inc., New York, 1941.

16 C. F. Bohren and D. R. Huffman, *Absorption and Scattering of Light by Small Particles*, *2nd* ed. Wiley-Interscience, New York, 1998.

17 Y. Liu, M. Gibbs, J. Puthussery, S. Gaik, R. Ihly, H. W. Hillhouse and M. Law, *Nano Lett*., 2010, **10**, 1960.

18 M. O. Sinnokrot, E. F. Valeev and C. D. Sherrill, *J. Am. Chem. Soc.*, 2002, **124**, 10887.

19 K. Park, H. Koerner and R. A. Vaia, *Nano Lett*., 2010, **10**, 1433.

Table of Contents Graphic and Synopsis

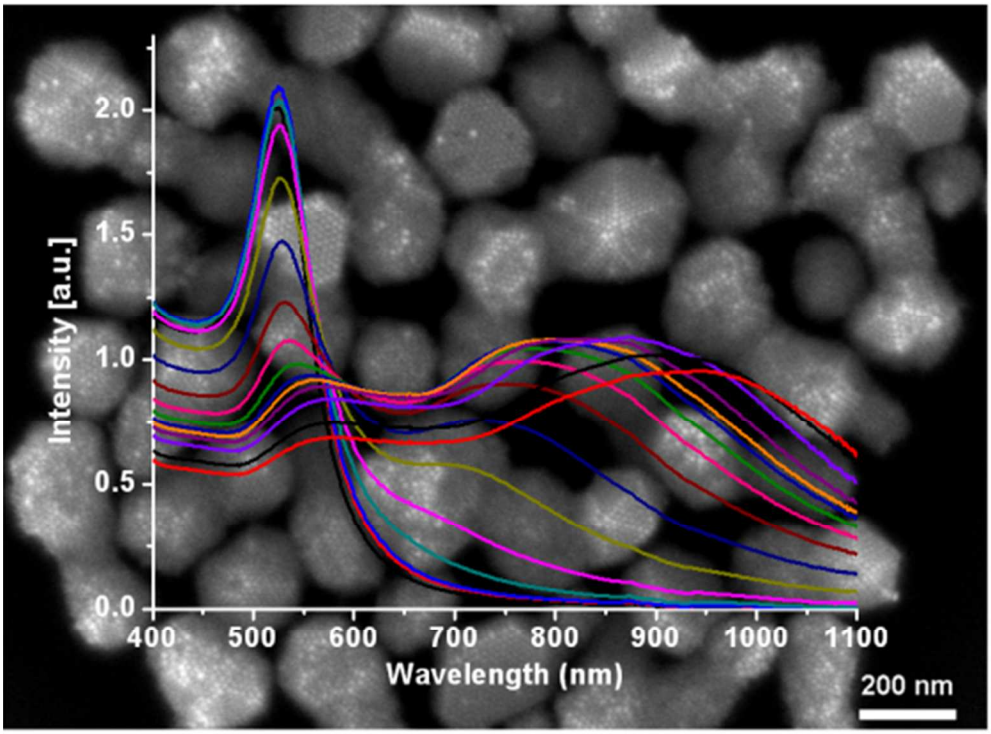

Here we present the first attempt to employ π-π interactions to assemble gold nanoparicles into single crystalline superlattices in solution. Simple capping ligands exchange with aromatic thiol lead self-assembly to gold nanoparticles into *fcc* packed superlattices with defined facted structures in solution. The long-range ordering was confirmed by TEM analysis and in situ UV-vis NIR spectra. Stimuli that can break the π-π interactions would lead to a reversible disassembly, allowing the design of reversible assembly of gold nanoparticles or reconfigure in response to external stimuli. In addition, the crystallization is kinetically controlled by the concentration of aromatic thiols in solution. The π-π interaction and depletion force work together to tune the long-range and short-range ordering in the resulting nanoparticles lattices, together with tailable collective plasmonic extinction.